https://doi.org/10.17221/265/2020-CJFS

# Extrusion rheometry of collagen dough

*Jan Štípek*, Jan Skočilas, Jaroslav Štancl, Rudolf Žitný*

*Department of Process Engineering, Faculty of Mechanical Engineering, Czech Technical University in Prague, Prague, Czech Republic*

**Corresponding author: jan.stipek@fs.cvut.cz*

**Citation:** Štípek J., Skočilas J., Štancl J., Žitný R. (2021): Extrusion rheometry of collagen dough. Czech J. Food Sci., 39: 384–392.

**Abstract:** Although collagen is widely used (for example, in the food industry, in the pharmaceutical industry and in biomedicine), the rheological properties of the material are not well known for high concentrations (8% collagen, 90% water). Rheological properties were measured using a capillary-slit rheometer (an extrusion process), where the tested sample of collagen matter was pushed by a hydraulically driven piston through a narrow rectangular slit at very high shear rates of 50–6 000 $s^{-1}$. The Herschel-Bulkley (HB) constitutive equation and a new correlation taking into account the finite gap width was used to evaluate the rheological properties ($n$ = 0.2, $K$ = 879 Pa $s^n$, $\tau_0$ = 2 380 Pa). Use was made of a new yield stress measurement method evaluating $\tau_0$ 'post mortem' after extrusion stops. The effects of wall slip and of air bubbles, which caused apparent compressibility of the 'silly putty' collagen material, were also studied. Corrections of the wall slip effect were implemented using sliding layer thickness δ.

**Keywords:** compressibility; Herschel-Bulkley; rheometer; wall slip; yield stress

Collagen material with a high concentration of the collagen component has already found applications in various fields, such as additive manufacturing (Mackay 2018), medicine (Kumar et al. 2013), and the food industry (Barbut et al. 2020). The sensory properties and the structure of highly concentrated collagen matter resemble those of bread dough. Methods of bread dough rheology include linear viscoelasticity [small amplitude oscillatory shear (SAOS)], measurements of yield stress, relaxation tests and capillary extrusion (Sofou et al. 2008). Bread dough integral models [Kaye-Bernstein, Kearsley, Zapas (KBKZ)] with damage functions are able to describe large amplitude oscillation shear (LAOS) (Tanner et al. 2006, 2008). All of these methods could probably be used for collagen (Barnes et al. 1989; Steffe 1996; Tanner 2000). Because of the discharge of tested collagen samples from the gap between the plates, and because of slip wall effects, rotational rheometers can be used only in studies of small deformations (Houška et al. 2016). Rheological properties at much higher shear rates can be evaluated using extrusion slit rheometers (Skočilas 2016). This paper extends previous results and suggests new experimental methods and physical models (yield stress, compressibility).

## MATERIAL AND METHODS

**The tested material.** The material tested in this study was a collagen water dispersion with 7.7% mass fraction of bovine collagen. The tested collagen is used for sausage casings in the food industry. The material was stored in a cooling room with evaporator to prevent degradation. The measurements were performed at a constant temperature of the material (9 ± 1 °C).

**Extrusional rheometer setup.** The slit-capillary rheometer (constructed at the Czech Technical University in Prague, Department of Process Engineering) used in the tests was developed for batch extrusion of dough-like plastic materials through a die with a rectangular cross-section (width $W$ = 20 mm, variable thickness

Supported by the Student grant competition (SGS) program (Project No. SGS20/118/OHK2/2T/12) and by the Grant agency of the Czech Republic (No. 21-07851S)

https://doi.org/10.17221/265/2020-CJFS

of gap $H$ = 2, 4, 8 mm, length $L$ = 200 mm). The experimental setup of the rheometer is shown in Figure 1. The sample of collagen dispersion is pushed through the capillary from a cylindrical container using a hydraulically-driven piston ($D$ = 80 mm). The piston speed is manually adjusted up to approximately 0.038 m $s^{-1}$. Variation of the shear rate by almost three orders can be achieved ($\Gamma \sim u_{piston}/H^2$, 50–6 000 $s^{-1}$). The pressures were measured by 6 flush-mounted XPM4 transducers (TE Conectivity, Berwyn, Illinois, USA), which are calibrated by the manufacturer against atmospheric pressure. All pressure values mentioned later are considered with respect to atmospheric pressure. The WPS-500 potentiometer (Micro-Epsilon, Bechyne, Czech Republic) monitors the position of the piston, from which the speed of the piston is computed. All sensors were connected to the QuantumX MX840B data acquisition system (HBM, Brno, Czech Republic) and were recorded using LabView 2014, v14.0. The result of each experiment is summarised in the chart (Figure 2), where the pressure-time dependence and the piston displacement are displayed. Approximately ten experiments were performed for each tested geometry. All overpressure values are zero in the first phase

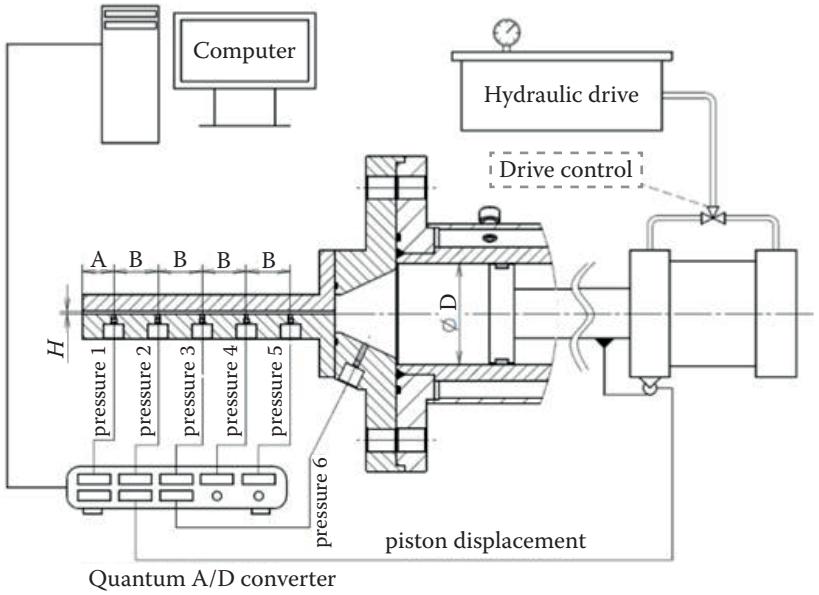


Figure 1. Model of the capillary rheometer and its connection to the measuring system

Gap $H$ = 2, 4, 8 mm, A = 25 mm, B = 35 mm, D = 80 mm; the capillary length (200 mm) and width (20 mm) is the same for all capillary heights

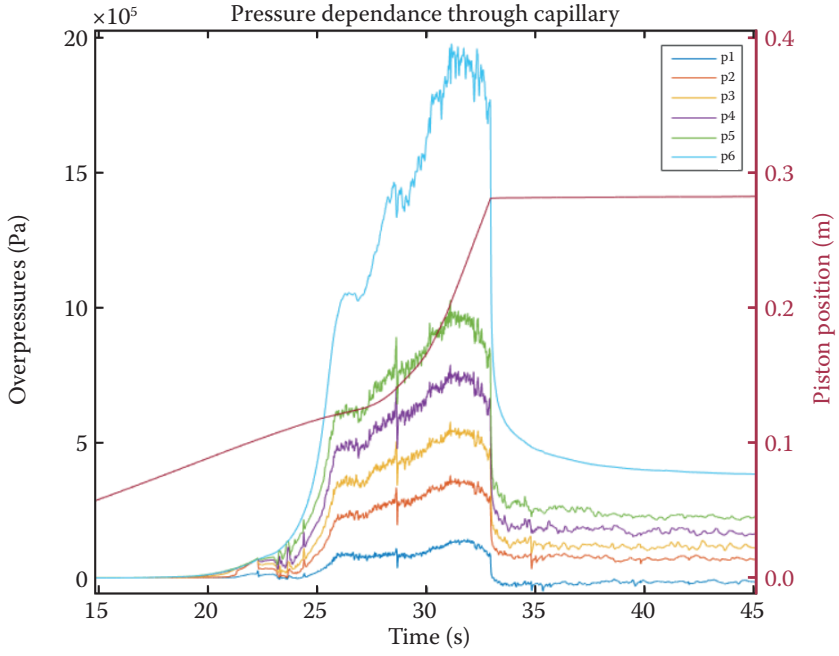


Figure 2. Time dependence of the overpressure recorded by 6 pressure transducers including the piston displacement (capillary $H$ = 4 mm)

https://doi.org/10.17221/265/2020-CJFS

of the experiment ($t$ < 20 s; the absolute time values are not important). There is a rapid increase of pressures at time $t \cong 25$ s, when the piston comes into contact with the collagen matter. The subsequent steady increase in pressures (between $t$ = 27 s and $t$ = 33 s) is caused by the increasing speed of the piston and was to be expected. There is a surprisingly high noise level. This is not caused by the pressure sensors themselves but by the presence of air bubbles. The existence of air bubbles is mainly responsible for the phenomena observed after the piston comes to a stop. The piston stops almost immediately (in milliseconds), without any inertial effects (Figure 2), but the collagen expression continues, as can be observed visually. The outflow is accompanied by the recorded relaxation of pressures. However, the pressures do not relax to the value of the atmospheric pressure, but to slightly higher values, as if some residual internal stresses had been generated.

**Power (*K, n* identification).** The basic rheological properties were described by the power law (PL) constitutive equation:

$$\tau = K\dot{\gamma}^n \tag{1}$$

where: τ – shear stress (Pa); $\dot{\gamma}$ – shear rate ($s^{-1}$); $n$ (–) and $K$ (Pa $s^n$) – flow index and coefficient of consistency (PL model constants).

The PL model (Equation 1) can be used to provide a description of the relationship between directly measured properties, the flow rate $\dot{V}$ and the axial gradient of pressure $\partial p/\partial z$ for fully developed laminar flow through a rectangular cross-section (width $W$, height $H$):

$$\dot{V} = \frac{2n}{2n+1}\left(\frac{\partial p}{K\partial z}\left(1-\frac{192}{\pi^5}\frac{H}{W}\right)\right)^{\frac{1}{n}}\left(\frac{H}{2}\right)^{\frac{2n+1}{n}} W \tag{2}$$

where: $\dot{V}$ – flow rate; $p$ – pressure; $z$ – axis of flow direction; $H$ – thickness of gap; $W$ – width of gap.

The Rabinowitsch, Mooney, Weissenberg equation (Equation 2) is a more or less standard PL model. The equation follows from *per partes* integration of the flow rate, assuming a linear transversal shear stress profile, $t = 2\tau_w y/H$, e.g. Steffe (1996). The correction term $[1–(192H/W\pi^5)]$ representing the effect of finite width $W$ was inspired by the analytical solution of a Newtonian fluid. This correction was carefully tested by a numerical finite differences method [alternating-direction implicit (ADI) method] for a broad range of flow behaviour index $n \in (0.2, 1.0)$ and $H/W \in (0.0, 0.4)$. Within this range (ratio $H/W < 0.4$), the error of the calculated flow rate is typically less than 1%, while, for example, at $H/W = 1$ (square) and $n = 0.3$ the error increases to 59%.

The primary data (time, piston displacement and overpressures $p_1, p_2, \ldots, p_6$) were transformed into Matlab R2015. No filtering was used for evaluating the rheological properties $K$, $n$ of the PL model. This was an easy task because Equation 2 is represented by a straight line in a graph of logarithms of consistency variables (Γ is the shear rate at the wall for a Newtonian liquid, and the wall shear stress $\tau_w$ follows from the equilibrium of forces). The slope of this line is the flow index $n$, and consistency $K$ can be calculated from $n$:

$$\tau_w = K\Gamma^n\left(\frac{2n+1}{n}\right)^n = K\dot{\gamma}_w^n \tag{3}$$

$$n\log\Gamma = n\log\frac{n}{2n+1} - \log K + \log\tau_w \tag{4}$$

$$\Gamma = \frac{2\dot{V}}{H^2 W}$$
$$\tau_w = \frac{dp}{dz}\frac{H}{2}\left(1-\frac{192}{\pi^5}\frac{H}{W}\right) \cong \frac{p-p_e}{L}\frac{H}{2}\left(1-\frac{192}{\pi^5}\frac{H}{W}\right) \tag{5}$$

where: $\tau_w$ – wall shear stress; Γ – shear rate at the wall for a Newtonian liquid; $\dot{\gamma}_w$ – wall shear rate; $p_e$ – exit pressure; $L$ – capillary length.

The consistency variable Γ (and the wall shear rate $\dot{\gamma}_w$) can be recalculated from the recorded velocity of the piston as soon as the collagen material becomes incompressible. This is not an exact statement due to the presence of air bubbles. This distortion can be neglected when the velocity can be assumed to be constant and when the displacement can be considered as quasi-static. The dynamic consistency variable $\tau_w$ can be calculated from simultaneously recorded overpressures $p_1, \ldots, p_5$, assuming a linear axial profile of the pressure. Distortions due to the compressibility of the collagen material, the end and the wall slip effects or insufficiencies of the assumed PL rheological model are possible explanations of inconsistencies visible in the graph of consistency variables Γ, $\tau_w$, because the experimentally determined function $\tau_w(\Gamma)$ should be independent of geometry, i.e. independent of gap thickness $H$.

**The Herschel-Bulkley (HB) yield stress (residual stresses).** Let us return to Figure 2. The active phase

https://doi.org/10.17221/265/2020-CJFS

of the extrusion ends when the piston stops (approximately at time $t$ = 33 s) and when the overpressures $p_{stop}$, shown in the second row of Table 1, are at their maximum. Afterwards, the pressures relax, but not to zero overpressure (atmospheric pressure). About ten seconds later ($t$ = 46 s), the relaxed and almost constant overpressures $p_{rel}$ are given in the third row of the table. The fourth row presents the distance $L$ of the corresponding pressure transducers from the exit of the channel, where atmospheric pressure is assumed. It is hypothesised that the non-zero equilibrium overpressures $p_{res}$ correspond to the yield stress of the collagen $\tau_0$, which is the same as the wall shear stress $\tau_w$ at equilibrium. When the motion stops, the rate of deformation $\dot{\gamma}$ will be zero, and the collagen material remaining in the container and in the capillary behaves like an elastic compressible solid. The equilibrium of forces in the axial direction can be expressed as $p(x)WH/2 = \tau_w WL(x)$, where $L(x)$ is the distance from the location of the pressure transducer to the exit of the capillary. Assuming a linear axial pressure profile, and therefore assuming constant wall shear stress, the yield shear stress can be estimated from the relaxed pressures of all six pressure transducers as:

$$\tau_0 = p(x)\frac{H}{2L(x)} \tag{6}$$

These calculated values are displayed in the last row of Table 1. Table 1 presents only one typical experiment. However, the conclusion that $\tau_0$ is almost constant along the whole capillary was confirmed by all experiments and for all dimensions of the capillary ($H$ = 2, 4, 8 mm). Equation 6 is probably the simplest method for experimentally making an estimate of the yield stress. The existence of very high non-zero yield stress ($\tau_0 \cong$ 3 000 Pa) has consequences concerning the evaluation of the hydraulic characteristic during flow. Instead of the PL model (Equation 1), the HB constitutive equation should be used:

$$\tau = \tau_0 + K\dot{\gamma}^n \tag{7}$$

The hydraulic characteristic (the flow rate as a function of the pressure gradient) can be derived using the same method of per partes integration of the flow rate integral Equation 2, giving:

$$\dot{V} = \frac{WH^2}{2}\frac{n}{2n+1}\left(\frac{\tau_w}{K}\right)^{\frac{1}{n}}\left(1-\frac{\tau_0}{\tau_w}\right)^{\frac{n+1}{n}}\left(1+\frac{n}{n+1}\frac{\tau_0}{\tau_w}\right) \tag{8}$$

The graph of constitutive variables $\Gamma$ and $\tau_w$ follows from Equation 8, preserving the definitions (Equation 5):

$$\Gamma^n = \left(\frac{n}{2n+1}\right)^n \frac{\tau_{wcorr}}{K}$$
$$\tau_{wcorr} = \tau_w\left(1-\frac{\tau_0}{\tau_w}\right)^{n+1}\left(1+\frac{n}{n+1}\frac{\tau_0}{\tau_w}\right)^n \tag{9}$$

$$n\log\Gamma = n\log\frac{n}{2n+1} - \log K + \log\tau_w + \left(n+1\right)\log\left(1-\frac{\tau_0}{\tau_w}\right) + n\log\left(1+\frac{n}{n+1}\frac{\tau_0}{\tau_w}\right) \tag{10}$$

The graph of consistency variables $\Gamma$ and $\tau_w$ is no longer a straight line, and non-linear regression must be used to identify the HB model ($K$, $n$, $\tau_0$). Fortunately, only a small number of iterations are sufficient for $\tau_{wcorr}$ calculated according to Equation 9 from the known yield stresses $\tau_0$ and from the previous iteration of flow behaviour index $n$.

**Compressibility and relaxation of pressures.** The experiments represented in Figure 2 indicate apparent compressibility of the tested collagen material in all phases of the experimental run (cavity filling, gradually increasing extrusion, and the stopping of the driven piston). However, the collagen itself is practically incompressible (more than 90% is water, and our own special experiment using very high pressures

Table 1. Example of yield stress evaluation

| Pressure transducer | P1 | P2 | P3 | P4 | P5 | P6 |
|---|---|---|---|---|---|---|
| $p_{stop}$ (MPa) | 0.08 | 0.29 | 0.44 | 0.61 | 0.79 | 1.73 |
| $p_{rel}$ (MPa) | 0 | 0.07 | 0.12 | 0.17 | 0.22 | 0.38 |
| $L$ (mm) | 25 | 60 | 95 | 130 | 165 | 250 |
| $pH/(2L)$ (MPa) | 0.0000 | 0.0023 | 0.0025 | 0.0026 | 0.0027 | 0.0030 |

Data in the table represent Figure 2 ($H$ = 4 mm); pressure values obtained after the piston stopped: $p_{stop}$ – pressure value at the moment of piston stoppage; $p_{rel}$ – pressure value after the creation of equilibrium; $L$ – distance of the pressure transducer from the capillary exit; $pH/(2L)$ – value corresponding to the yield stress according to Equation 6

https://doi.org/10.17221/265/2020-CJFS

confirms incompressibility). The problem lies in the air, which is almost always present in the processed collagen dough (e.g. due to mixing). Instead of characterising the material as an incompressible liquid, it is necessary to characterise it as a two-phase system of incompressible collagen (liquid) and dispersed tiny bubbles of air (gas). The simplest idea assumes the existence of a single big bubble enclosed in a cavity between the moving piston and the moving surface of the collagen (Figure 3). This approach is simple and is probably more realistic than the assumption of dispersed tiny air bubbles throughout the rheometer. It corresponds to the preparation of an experiment in which the container is first manually filled with collagen and then closed by the piston. There is no vacuum pump and no other arrangement for removing air below the piston, and it is assumed that most of the air escapes through the sealing of the piston. The primary aim of the analysis is to estimate the deviation between the velocity of the piston ($u_p$ which is directly and quite accurately measured) and the velocity of the extruded collagen. The analysis is based on the continuity equation, which states that the actual volume of the container $V(t)$ is the sum of the volume occupied by pure and incompressible collagen $V_c$ and the volume of air $V_a$, which has a constant mass $M_a$ (assuming no escape through the piston sealing). Using the ideal state equation for the air and assuming a constant temperature $T_a$, the volume of air bubble $V_a$ is only a function of the overpressure $p_a$ plus the atmospheric pressure $p_{0:}$

$$V_a(t) = \frac{R_a T_a M_a}{p_a(t) + p_0} \tag{11}$$

where: $V_a$ – volume of air; $R_a$ – individual gas constant for air; $T_a$ – constant temperature; $M_a$ – constant mass; $p_a$ – overpressure; $p_0$ – atmospheric pressure.

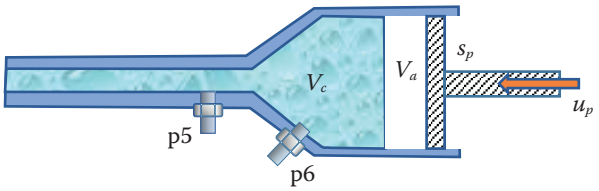


Figure 3. Model of the two-phase system (air and collagen)

$u_p$ – piston speed; $S_p$ – piston area; $V_c$ – volume of collagen; $V_a$ – volume of air; pressure transducers detecting the pressure in the reservoir area ($p_6$) and at the entrance to the capillary ($p_5$)

The overpressure $p_a$ can be approximately identified with the $p_6(t)$ recorded by the pressure transducer. $R_a$ is the individual gas constant for air [J(kg K)$^{-1}$]. The continuity equation reduces to:

$$S_p u_p(t) = \dot{V}_c(\tau_w) + \frac{dV_a}{dt} = \\ = \dot{V}_c(\tau_w) - \frac{R_a T_a M_a}{\left(p_a(t) + p_0\right)^2} \frac{dp_a}{dt} \tag{12}$$

where: $S_p$ – piston area; $u_p$ – speed of the piston; $V_c$ – volume occupied by pure and incompressible collagen.

The volumetric collagen flow rate is determined by the measured axial pressure gradient and by the related wall shear stress, according to Equation 8, which can therefore be expressed in terms of constitutive variables, and by using Equation 9 for $\tau_{wcorr}$:

$$\Gamma(t) = S_p u_p(t) \frac{2}{H^2 W} = \frac{n}{2n+1} \left( \frac{\tau_{wcorr}}{K} \right)^{\frac{1}{n}} - \\ - \frac{\psi_a}{\left(p_a(t) + p_0\right)^2} \frac{dp_a}{dt} \tag{13}$$

where: $\Psi_a$ – potential energy of the compressed air (J m$^{-3}$) is expressed as:

$$\psi_a = \frac{2 R_a T_a M_a}{H^2 W} \tag{14}$$

The mass $M_a$ of the air bubble is not known in advance, and its value has nothing to do with the investigated properties of the collagen. The presence of air bubbles is an instrumental distortion that cannot be eliminated simply. The only way to eliminate the distortion is to estimate the corresponding damage and the magnitude of the errors in the calculated Γ. Equation 13 clearly indicates that the compressibility errors are small at an almost constant velocity of the extrusion and at high pressures in the container. The order of this correction can be calculated from the overpressures $p_{1,2,3,4,5}$ ($\tau_{wcorr,\ stop}$) and $p_6$ recorded after the piston has stopped (Γ = 0):

$$\psi_a = \frac{n}{2n+1} \left( \frac{\tau_{wcorr,stop}}{K} \right)^{\frac{1}{n}} \frac{\left(p_{6,stop} + p_0\right)^2}{\frac{dp_{6,stop}}{dt}} \tag{15}$$

The correction of flow rate according to Equation 13 is an example of scale up – it is not necessary to know the actual mass $M_a$.

https://doi.org/10.17221/265/2020-CJFS

**Wall slip.** The discrepancy represented by the non-unique representation of the function $\tau_w(\Gamma)$, which should be independent of $H$, is usually attributed to the wall slip effect. It is assumed that at high wall shear stresses or at a high wall shear rate, the tested material (collagen) will separate from the wall and will slip as a solid layer at a velocity of $u_s$. The hydraulic characteristic (Equation 8) for an HB liquid should be modified to:

$$\Gamma = \frac{2\overline{u}}{H} = \frac{2u_s}{H} + \frac{n}{2n+1}\left(\frac{\tau_{wcorr}}{K}\right)^{1/n} \quad (16)$$

where: $\overline{u}$ – mean velocity, defined as $\overline{u} = \dot{V}/(WH)$.

The rate of deformation Γ (calculated from the measured flow rate) is decomposed to the unknown contribution of the slip and to the contribution of the transversal velocity profile according to the Rabinowitsch equation. The slip velocity is usually assumed to be proportional to the wall shear stress:

$$\Gamma = \frac{2\beta\tau_{wcorr}}{H} + \frac{n}{2n+1}\left(\frac{\tau_{wcorr}}{K}\right)^{1/n} \quad (17)$$

This equation is usually used for an evaluation of the slip coefficient β using the Mooney graph, where the horizontal axis is $1/H$ ($m^{-1}$) and the vertical axis is Γ ($s^{-1}$). The slip coefficient β is represented by the slope of the constant wall shear stress $\tau_{wcorr}$ lines in this diagram. The slip coefficient β is, in fact, a function of the wall shear stress that can be arbitrary selected within the overlapping range of measured $\tau_{wcorr}$. Another way to model the slip is to introduce a critical load, after which the collagen layer will tear off the wall. An extreme simplification is the idea of a thin sliding layer of constant thickness δ. Adding this layer to the channel thickness of gap $H$ will increase the flow rate. This correction is significant only for narrow slits (as it should be).

$$\Gamma = \frac{2\overline{u}}{H+\delta} \quad (18)$$

## RESULTS AND DISCUSSION

The rheological parameters of the PL and HB models $K$, $n$, mean yield stress $\tau_0$, and the energy of the compressed air $\Psi_a$ are calculated using Matlab script and primary data. Experimental points consisting of measured flow rates $\dot{V}_i$ (more accurately $S_p u_{pi}$) and the axial pressure gradient $(dp/dz)_i$ are recalculated to the consistency variables $\Gamma_i$, $\tau_{wi}$ and are plotted in Figure 4–6. Circles and red colour correspond to $H$ = 2 mm; squares and green colour correspond to $H$ = 4 mm, and triangles and blue colour correspond to the capillary $H$ = 8 mm. Thick lines represent the HB model, and thin lines represent the PL model. The lines are overlapped most of the time. The figures contain the same experimental data but are presented using different models or transformation of consistency variables. Figure 4 calculates the wall shear stress, assuming an infinitely wide slit (H/W → 0)

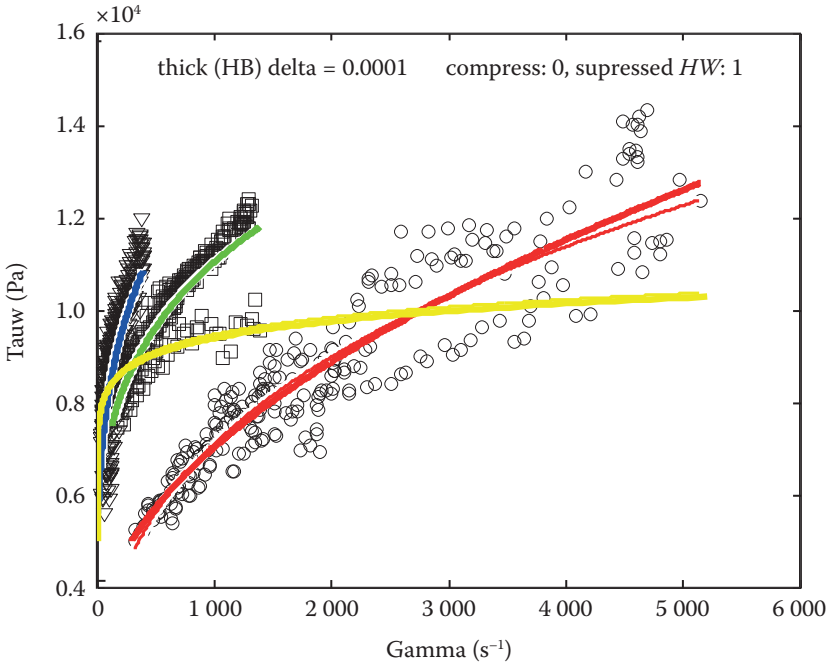


Figure 4. Rheogram displaying the values ($\tau_w$ – Γ calculated from the pressure dependence) for $H$ = 2 mm (values represented by circles and fitted with a red line), $H$ = 4 mm (values represented by squares and green line), $H$ = 8 mm (values represented by triangles and blue line) and all data combined (yellow line), using a compressed model, assuming infinite capillary width $W$ and using a small value of delta (Equation 18) to reduce the wall slip effect

Data are fitted with two models: power law (PL) (thin line) and Herschel-Bulkley (HB) (thick line)

https://doi.org/10.17221/265/2020-CJFS

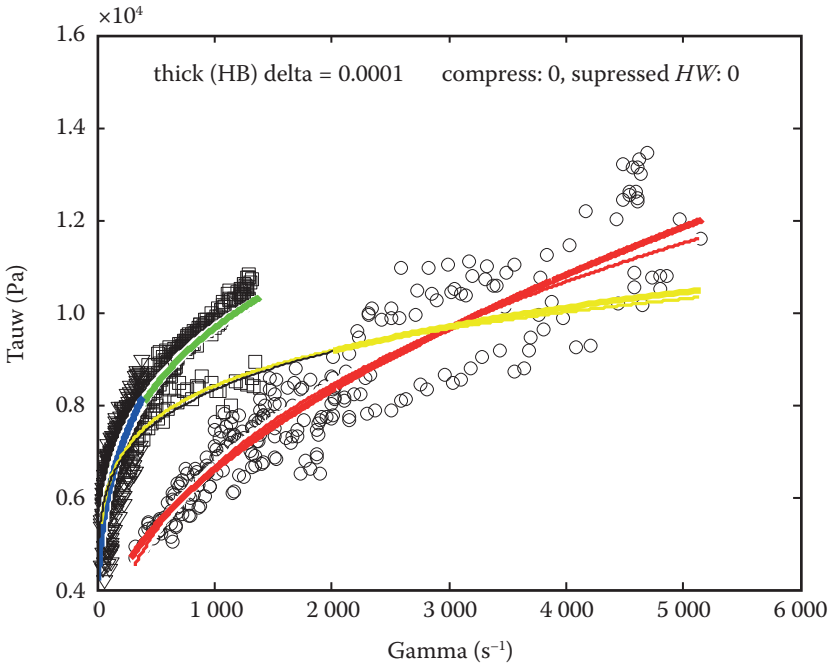


Figure 5. Rheogram displaying the values ($\tau_w$ – Γ calculated from the pressure dependence) for $H$ = 2 mm (values represented by circles and fitted with a red line), $H$ = 4 mm (values represented by squares and green line), $H$ = 8 mm (values represented by triangles and blue line) and all data combined (yellow line), using a compressed model taking into account the impact of the finite width of the capillary and using a small value of delta (Equation 18) to reduce the wall slip effect

Data are fitted with two models: power law (PL) (thin line) and Herschel-Bulkley (HB) (thick line)

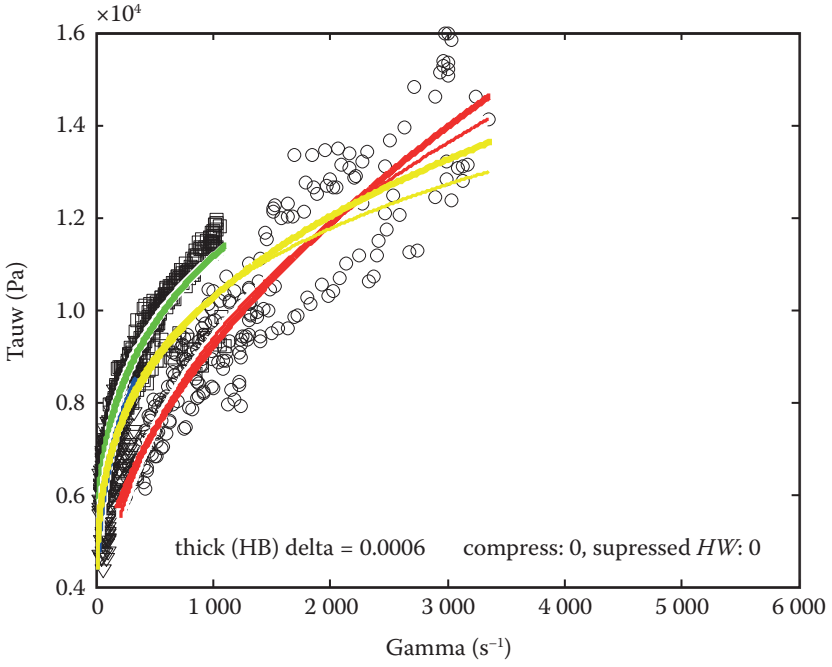


Figure 6. Rheogram displaying the values ($\tau_w$ – Γ calculated from the pressure dependence) for $H$ = 2 mm (values represented by circles and fitted with a red line), $H$ = 4 mm (values represented by squares and green line), $H$ = 8 mm (values represented by triangles and blue line) and all data combined (yellow line) using a compressed model taking into account the impact of the finite width of the capillary and using bigger values of delta (Equation 18) to reduce the wall slip effect

Data are fitted with two models: power law (PL) (thin line) and Herschel-Bulkley (HB) (thick line)

and therefore neglecting the shear stresses acting at the lateral sides of the cross-section. The corresponding correction of the $H/W$ ratio (used for Figure 5 and 6) is represented by the coefficient $[1–(192H/W\pi^5)]$, used in Equation 2. Compression of the air bubble according to Equation 13 and 15 is used in all of these figures. There is another obvious significant difference between Figure 5 and 6. These figures differ in the value used for δ for the wall slip corrections. The value is negligible in Figure 5, whereas in Figure 6 the value of δ = 0.006 mm significantly affects the rheogram. Some conclusions can be drawn from these figures. A negative conclusion is that the tested general Newtonian glow (GNF) model does not fit a unique relationship between consistency variables (and it does not matter whether the PL model or the HB model is used). The correction for a finite $H/W$ ratio improves the discrepancy, but only slightly (the differences between functions $\tau_w(\Gamma)$

https://doi.org/10.17221/265/2020-CJFS

for $H$ = 2, 4, 8 mm are smaller). The finite $H/W$ correction is important for $H/W$ > 0.1 and significantly improves the results for $H/W$ = 0.2 ($H$ = 4 mm) and 0.4 ($H$ = 8 mm), in agreement with numerical simulation using the finite difference method (alternating direction implicit). It seems that the experiments with the smallest gap $H$ = 2 mm ($H/W$ = 0.1) are affected by something else, for example, by a wall slip. The effect of air bubbles is probably innocent in this case (although the effect of bubbles is significant and reduces the Γ values considerably at low shear rates). A positive finding concerns the yield stresses: although the points in the diagram of consistency variables exhibit very high scatter, the evaluated yield stresses are almost constant. The dynamically determined yield stress $\tau_0$ can therefore be considered as a real material parameter independent of geometry. This value is quite high, between 2 000 Pa and 3 000 Pa, and the yield stress therefore explains about one-third of the wall shear stresses. Continuous lines in the figures $\tau_w$ (Γ) represent the predictions of the PL model and the HB model defined by parameters $n$, $K$, and $\tau_0$. The yield stress $\tau_0$ is determined directly, using the residual stresses recorded long after extrusion, and parameters $K$, $n$ are determined by regression analysis applied to the axial pressure profiles recorded during the active phase of the experiment (extrusion). Regression analysis is, in fact, performed twice, once assuming zero yield stress and then assuming independently determined and fixed $\tau_0$. We think that our findings show that the second statement is true and that the yield stress $\tau_0$ is not a fiction but a reality. The results from Matlab are displayed in Table 2. Parameters $K$ and $n$ are not calculated as an average of the values evaluated by regression of individual experiments but as a result of regression applied to all primary data from repeated experiments (4 885 data points from 6 experiments at $H$ = 2 mm). The last row in Table 2 is also not calculated as the mean values of 3 × 6 experiments. It was obtained as a result of regression applied to all 11 062 aggregated points in Figure 5. Please note, however, that the results in Table 2 are valid only for very small δ. Values $K$ and $n$ from aggregated points are outside the range of results corresponding to a different geometry, which is a direct consequence of a wall slip. The only exception is the yield stress $\tau_0$, where the mean value of 2 380 Pa is within the range of values for different H.

The validity range of the shear rate is provided, and also the shortest residence times corresponding to the maximum velocity. The residence time of an air bubble passing through the capillary (of the order 0.1 s) is so short that it cannot be accurately resolved by the pressure transducers at a sampling frequency of 100 Hz. However, this value could be important when analysing the expansion of the bubble near the end of the capillary. The 'exit pressure' was found to be almost zero during the experiments. For that reason, no viscoelastic models were used. The presence of air bubbles may create an apparent swell effect.

To the best of the knowledge of the authors, there has been no published article dealing with the evaluation of collagen material with such a high collagen mass fraction. Collagen has been examined at lower concentrations in the past when the structure is more liquid, and the material can therefore be tested using rotational rheometers (Micutz et al. 2015; Weiss et al. 2015). Similar experiments to those published in this paper have been carried out with collagen dough using capillary and slit rheometers (Skočilas et al. 2016). The evaluation technique and the evaluated rheological properties were similar. The following recently published papers dealing with collagen should be mentioned: both Demeter et al. (2020) and Li et al. (2020) use dynamic rheological measurements. In addition, thermal stability and improvements of viscoelasticity were tested using cross-linking of collagen fibrils (Li et al. 2020). It is crucial to understand the behaviour of viscoelastic materials for the engineering design

Table 2. Rheological parameters evaluated from data points in Figure 5 with obvious wall slip consequences resulting from the small parameter δ that was used

| $H$ (mm) | *ndat* | $n_P$ | $K_p$ (Pa s$^n$) | $n_{HB}$ | $K_{HB}$ (Pa s$^n$) | $\tau_0$ (Pa) | Γ (s$^{-1}$) | $t_{RTD}$ (s) |
|---|---|---|---|---|---|---|---|---|
| 2 | 4 885 | 0.272 | 644 | 0.417 | 123 | 2 140 ± 118 | 180 – 5 800 | 0.04 |
| 4 | 3 106 | 0.161 | 2 180 | 0.243 | 771 | 2 505 ± 133 | 150 – 1 500 | 0.07 |
| 8 | 3 071 | 0.155 | 2 090 | 0.304 | 415 | 2 820 ± 628 | 27 – 410 | 0.12 |
| 2 + 4 + 8 | 11 062 | 0.126 | 2 490 | 0.200 | 879 | 2 380 | 27 – 5 800 | – |

$H$ – variable thickness of capillary gap; *ndat* – amount of data used for the evaluation; $n_p$ and $n_{HB}$ – power law (PL) and Herschel-Bulkley (HB) flow index, $K_p$ and $K_{HB}$ – PL and HB coefficient of consistency, $\tau_0$ – yield stress, $t_{RTD}$ – residence time, Γ – shear rate

https://doi.org/10.17221/265/2020-CJFS

of machines working with such materials. Collagen is very often used as a component in materials for tissue engineering, sometimes 3D printed, as described by (Shibli et al. 2021). These articles show that there are various applications of collagen. However, as has already been mentioned, there are no published articles dealing with the rheological properties of such highly concentrated collagen matter.

## CONCLUSION

The purpose of this study was to evaluate the rheological properties of concentrated collagen material. The tested samples of bovine collagen have a structure similar to that of dough, and they seem to act more like a solid material than a liquid. An extrusion slit rheometer was chosen for the experiments because we set out to explore the behaviour of collagen material at high shear rates when the tested material behaves like a liquid. Collagen was measured on 3 different geometries (3 rectangular slits with different heights) of the extrusion heads. The rheological properties of the measured material were evaluated in Matlab using the HB model, taking into account the finite width of the rectangular cross-section and the compressibility. We tested a method for reducing the wall slip effect using an apparent sliding layer. A new method for evaluating the dynamic yield stress was developed and tested. These findings should be helpful for an evaluation of the rheological parameters of viscoplastic materials. The effects of viscoplasticity are sometimes unwanted. Understanding some of the properties mentioned in this study can be helpful for reducing unwanted effects and lead to improvements to manufacturing processes, for example, in the jet design in 3D printing, where collagen is used as a component to replace tissues in printed materials. This paper has attempted to use established principles of extrusion rheometry and to find new ways to evaluate the data.

## REFERENCES

Barbut S., Ioi M., Marcone M. (2020): Co-extrusion of collagen casings. Effects of preparation, brining, and heating on strength, rheology and microstructure. Italian Journal of Food Science, 32: 91–106.

Barnes H.A., Hutton J.F., Walters K. (1989): An Introduction to Rheology. New York, USA, Elsevier Science Publishing Co.: 5–109.

Demeter M., Meltzer V., Călina I., Scărișoreanu A., Micutz M., Albu Kaya M.G. (2020): Highly elastic superabsorbent collagen/PVP/PAA/PEO hydrogels crosslinked via e-beam radiation. Radiation Physics and Chemistry, 174: 108898.

Houška M., Landfeld A., Skočilas J., Žitný R., Novotná P., Štancl J., Dostál M., Chvátil D. (2016): The effect of irradiation on rheological and electrical properties of collagen. Applied Rhelogy, 26: 43775.

Kumar V.A., Caves J.M., Haller C.A., Dai E., Liu L., Grainger S., Chaikof E.L. (2013): Acellular vascular grafts generated from collagen and elastin analogs. Acta Biomaterialia, 9: 8067–8074.

Li G., Tian Z., Shen L., Liu W. (2020): Construction of collagen gel with high viscoelasticity and thermal stability via combining cross-linking and dehydration. Journal of Biomedical Materials Research, 108: 1934–1943.

Mackay M.E. (2018): The importance of rheological behavior in the additive manufacturing technique material extrusion. Journal of Rheology, 62: 1549–1561.

Micutz M., Brazdaru L., Staicu T., Albu M., Sulea D., Leca M. (2015): Structural and rheological properties of collagen hydrogels containing tannic acid and chlorhexidine digluconate intended for topical applications. Comptes Rendus Chimie, 18: 160–169.

Shibli J.A., Saska S., Pilatti L., Blay A. (2021): Bioresorbable polymers: Advanced materials and 4D printing for tissue engineering. Polymers, 13: 563.

Skočilas J., Žitný R., Štancl J., Dostál M., Landfeld A., Houška M. (2016): Rheological properties of collagen matter predicted using an extrusion rheometer. Journal of Texture Studies, 47: 514–522.

Sofou S., Muliawan E.B., Hatzikiriakos S.G., Mitsoulis E. (2008): Rheological characterization and constitutive modeling of bread dough. Rheologica Acta, 47: 369–381.

Steffe J.F. (1996). Rheological Methods in Food Process Engineering. 2nd Ed. East Lansing, Michigan, USA, Freeman Press: 121–343.

Tanner R.I. (2000). Engineering Rheology. 2nd Ed. New York, USA, Oxford University Press: 19–152.

Tanner R.I., Dai S., Wang Ch. (2006): On the compressibility of bread dough. Korea-Australia Rheology Journal, 18: 127–131.

Tanner R.I., Qi F., Dai S. (2008): Bread dough rheology and recoil. Journal of Non-Newtonian Fluid Mechanics, 148: 33–40.

Weiss J., Oechsle A.M, Häupler M., Gibis M., Kohlus R. (2015): Modulation of the rheological properties and microstructure of collagen by addition of co-gelling proteins. Food Hydrocolloids, 49: 118–126.

Received: November 4, 2020
Accepted: July 20, 2021